DOI: 10.1021/ma1009879

Macromolecules
ARTICLE

Kinetically Controlled Self-Assembled Superstructures from Semicrystalline Chiral Block Copolymers

Chun-Ku Chen,[†] Shih-Chieh Lin,[†] Rong-Ming Ho,*[,†] Yeo-Wan Chiang,[‡] and Bernard Lotz[§]

[†]*Department of Chemical Engineering, National Tsing Hua University, Hsinchu 30013, Taiwan,* [‡]*Department of Materials and Optoelectronic Science, Center for Nanoscience and Nanotechnology, National Sun Yat-sen University, Kaohsiung 80424, Taiwan, and* [§]*Institut Charles Sadron, Centre National de la Recherche Scientifique, 23, Rue du Loess, B.P. 84047, 67034 Strasbourg, France*

Received May 4, 2010; Revised Manuscript Received August 4, 2010

ABSTRACT: Self-assembled superstructures resulting from the competition between crystallization and microphase separation of semicrystalline poly(styrene)-*b*-poly(L-lactide) (PS−PLLA) chiral block copolymers (BCPs*) were examined. A kinetically controlled process by changing nonsolvent addition rate was utilized to control the BCP* self-assembly. Single-crystal lozenge lamellae were obtained by the slow self-assembly (i.e., slow nonsolvent addition rate) of PS−PLLA BCP* with long PS chain (i.e., PS-rich PS−PLLA BCP*) whereas amorphous helical ribbon superstructures were obtained from the fast self-assembly (i.e., fast nonsolvent addition rate). Moreover, amorphous flat ribbon superstructures were obtained in achiral BCPs, poly(styrene)-*b*-poly(DL-lactide) (PS−PLA), suggesting that the chirality plays an important role in the formation of the helical ribbon superstructures. By contrast, the self-assembly of PS−PLLA BCP* with short PS chain (i.e., PLLA-rich PS−PLLA BCP*) was dominated by PLLA crystallization regardless of the variation of nonsolvent addition rate, indicating that the PLLA crystallization rate is dependent upon the length of PS chain in PS−PLLA BCPs*. As a result, the formation of helical architectures from the self-assembly of PS−PLLA BCP* reflects the impact of chirality on microphase separation, but the chiral effect might be overwhelmed by crystallization.

Introduction

In recent decades, the self-assembly of block copolymers (BCPs) has been widely studied because of their ability to self-assemble into one-, two-, or three-dimensional periodic nanostructures according to composition (i.e., volume fraction), which provides promising features in the field of nanotechnologies.[1−4] Various phases in bulk such as sphere (S), cylinder (C), gyroid (G), and lamellar (L) phases can be obtained through self-assembly because spatial segregation of thermodynamically incompatible blocks.[1−4] In addition to the formation of numerous BCP nanostructures in bulk, the self-assembly of BCPs can also be carried out in solution so as to create BCP aggregates with various morphologies. Eisenberg and co-workers synthesized a series of asymmetric poly(styrene)-*b*-poly(acrylic acid) amphiphilic BCPs and investigated their self-assembly in solution.[5−8] The BCPs favor a disordered state in a favorable solvent for both blocks. Subsequently, a selective solvent (i.e., water) was added to the BCP solution. Self-assembly takes place at some critical water content. Various equilibrium superstructures in solution such as spheres, rods, lamellae, vesicles, large compound micelles (LCM), and large compound vesicles (LCV) were obtained. These thermodynamic equilibrium superstructures in solution can be controlled by changing the BCP composition, the initial concentration of BCP solution, the amount of nonsolvent or selective solvent present in the solvent mixture, the nature of the solvent, and temperature. Lodge and co-workers found structural transitions from spheres to rods to vesicles in poly(styrene)-*b*-poly(dimethylsiloxane) BCP solution by changing the sole solvent selectivity.[9,10] Also, as the temperature was increased, the selectivity of the solvent decreased so that reverse structural transitions from vesicle to rod to sphere could be observed. The above results indicate that the observed structural transitions depend upon the thermodynamic interaction between solvent and the blocks in the BCPs.

Among self-assembled architectures, the helical morphology is probably the most fascinating one and has been extensively studied because of its specific function. The formation of helical morphologies was shown to have various origins.[11−19] The chirality of the compounds is of course the main origin. Nolte and co-workers[19] observed that helical superstructures could be obtained from the self-assembly of BCPs in the buffer solution of amphiphilic BCPs with a charged chiral block, such as poly(styrene)-*b*-poly(isocyano-L-alanine-L-alanine) and poly(styrene)-*b*-poly(isocyano-L-alanine-L-histidine) BCPs. Recently, a helical phase (H* phase) with hexagonally packed PLLA helices in a PS matrix was obtained in bulk by self-assembling poly(styrene)-*b*-poly(L-lactide) (PS−PLLA) with a PLLA volume fraction of 0.34 (i.e., $f_{PLLA}^{v} = 0.34$).[20] Also, a hexagonally packed core−shell cylinder phase with helical sense (CS* phase) could be found in PS−PLLA with $f_{PLLA}^{v} = 0.65$.[21] The PS microdomains are the shells, and the PLLA microdomains are the matrix and cores. The formation of these novel phases H* and CS* is attributed to the chiral effect on the self-assembly of BCPs so that this PS−PLLA BCP system was named chiral BCP (BCP*).[22]

The PLLA component is intrinsically a crystallizable polymer in view of its regular chiral configuration. Therefore, various interesting crystalline PS−PLLA nanostructures could be obtained by controlling the crystallization temperature of PLLA ($T_{c,PLLA}$) to create different conditions (i.e., under soft or hard confinement). The formation of crystalline helices in which PLLA crystallization directed by helical confined microdomain (i.e., under hard confinement) and crystalline cylinders in which

*To whom correspondence should be addressed: Tel 886-3-5738349; Fax 886-3-5715408; e-mail rmho@mx.nthu.edu.tw.

 Published on Web 08/16/2010

phase transformation of helical nanostructure dictated by crystallization (i.e., under soft confinement) occurred while $T_{c,PLLA} < T_{g,PS}$ (the glass transition temperature of PS) and $T_{c,PLLA} \geq T_{g,PS}$, respectively. As a result, the PLLA helical nanostructure in a PS matrix had a springlike behavior.[23,24] Apparently, the crystallization affects self-assembled nanostructures and creates different morphologies. The self-assembly of semicrystalline BCPs indeed gives rise to much more complicated morphologies than that of amorphous−amorphous BCPs because of the interplay of crystallization and microphase separation. The morphologies resulting from the combination and/or competition between crystallization and microphase separation of semicrystalline BCPs have attracted much attention in recent decades.[23−42]

For semicrystalline BCPs, the crystallization takes place in the amorphous melt below the equilibrium melt temperature but above the glass transition temperature T_g of the crystallizable block. By contrast, the microphase separation of BCPs takes place when cooling the disordered melt to below the order−disorder transition temperature (i.e., T_{ODT}) but above the T_gs of both blocks. Accordingly, the self-assembly of semicrystalline BCPs in bulk is supercooling dependent. By contrast, the formation of ordered textures from solution should be easier, since in addition it alleviates the chain entanglement problem. Also, manipulating the supersaturation (i.e., the concentration variation from saturated concentration in solution) can be employed to control the self-assembly process. In favorable cases, the self-assembly process can be followed under ambient conditions, and the resulting superstructures can be clearly isolated and identified. In this study, we investigate the competition between crystallization and microphase separation in the self-assembly of semicrystalline BCPs in solution. The solution of BCP chains is obtained by controlling the concentration below the critical micelle concentration (cmc). A nonsolvent is then introduced into the BCP solution to initiate the self-assembly. In this process, the variable is the rate of which the nonsolvent is added, which plays the same rule as the cooling rate in bulk crystallization. Our results indicate that the slow self-assembly (i.e., a slow nonsolvent addition rate) results in the formation of single-crystal lamellae whereas the fast self-assembly (i.e., a fast nonsolvent addition rate) gives rise to amorphous helical ribbons. It appears that the chiral effect is significant in the self-assembly of PS−PLLA BCP* through microphase separation, but it might be overwhelmed by crystallization.

Experimental Section

Materials. PS−PLLA BCPs* and PS−PLA BCP were prepared by a two-step living polymerization process. The synthetic routes, similar to our previous approach, are only briefly recalled here.[21] A double-headed initiator, $HOCH_2CH(CH_3)_2CH_2O-C(=O)CHCl(CH_3)$ (DHI4-Cl), was first prepared. Hydroxyl-terminated polystyrene (PS−OH) was then prepared by bulk atom transfer radical polymerization (ATRP) of styrene with DHI4-Cl as initiator and CuBr/HMTETA as catalyst/ligand. The PS−PLLA BCPs* and PS−PLA BCP were synthesized using the PS−OH as macroinitiator and $Sn(OCt)_2$ as catalyst for the ring-opening polymerization of L-lactide and DL-lactide to obtain PS−PLLA BCPs* and PS−PLA BCP, respectively. The PLLA homopolymer was also prepared by the ring-opening polymerization. The polymerization of the PLLA homopolymer was performed by using $Sn(Oct)_2$ as catalyst and benzyl alcohol (BnOH) as initiator. The molecular weight, volume fraction, and molecular weight distribution of the synthesized PS−PLLA BCPs* and PS−PLA BCP are listed in Table 1. On the basis of molecular weight and volume ratio, the PS−PLLA BCPs* are designated as PSx-PLAy ($f_{PLLA}{}^{v} = z$). Here x and y represent the number of repeating units for PS and PLLA blocks measured by NMR, respectively, and z indicates the volume fraction of PLLA calculated by assuming that the densities of PS and PLLA are 1.02 and 1.248 g/cm^3. The PS−PLA BCP is designated as PSx-PLAy ($f_{PLLA}{}^{v} = z$). The volume fraction of PLA was calculated by assuming density of PLA is 1.18 g/cm^3. The molecular weight distributions were characterized by GPC.

Table 1. Molecular Characterization of PS−PLLA BCPs* and PS−PLA BCP

sample	$M_{n,PS}$ (g mol^{-1})^a	$M_{n,PLLA}$ (g mol^{-1})^b	$f_{PLLA}{}^{v}$	PDI
PS272-PLLA118	28 300	17 000	0.33	1.21
PS55-PLLA95	6 000	13 900	0.65	1.17
sample	$M_{n,PS}$ (g mol^{-1})^a	$M_{n,PLA}$ (g mol^{-1})^b	$f_{PLA}{}^{v}$	PDI
PS355-PLA112	36 900	16 100	0.27	1.26

^{a} Obtained from GPC analysis. ^{b} Obtained from ^{1}H NMR measurement.

Sample Preparation. PS−PLLA BCPs* and PS−PLA BCP were first dissolved in tetrahydrofuran (THF). The initial polymer concentration in THF for all the samples was 0.1 wt %. Note that THF is a reasonably good solvent for both PS and PLLA blocks but slightly selective for the PS block. The solubility parameters of PS, PLLA, and THF are 18.8, 20.2, and 18.6 (MPa)$^{0.5}$, respectively.[43−45] PS−PLLA BCP* in THF solution can be prepared when the concentration is sufficiently low (see Supporting Information for details). Therefore, 0.1 wt % PS−PLLA/THF solutions were systematically employed. Subsequently, deionized water was added into the polymer/THF solution at either a slow or fast rate with stirring. After addition of water, the solubility of the BCPs decreased gradually, resulting in aggregation. The addition of water was carried out until the solution reached a preset supersaturation state (water content ~23% (v/v)) in all cases. Turbid solutions were obtained. When the deionized water is added dropwise at a slow rate (1.0% (v/v) per minute), the process is referred to as "slow self-assembly" (i.e., slow nonsolvent addition rate). For the higher rate (1.0% (v/v) per second), the process is referred to as "fast self-assembly" (i.e., fast nonsolvent addition rate). When reaching the 23% v/v concentration, the systems were immediately "quenched" by adding a large amount of deionized water to terminate the self-assembly and freeze in the resulting morphologies. Subsequently, the aggregates were dropped onto carbon-coated copper grids for TEM observation.

Transmission Electron Microscopy (TEM). Bright-field transmission electron microscopy (TEM) images were obtained using a JEOL JEM-2100 LaB_6 transmission electron microscope (at an accelerating voltage of 200 kV). Staining was accomplished by exposing the samples to the vapor of a 4% aqueous RuO_4 solution for 1 h. The RuO_4 attacks the double bonds in the PS blocks so as to increase the mass−thickness contrast for imaging.

Scanning Probe Microscopy (SPM). SPM images of the samples are taken in the tapping mode. A Seiko SPA-400 SPM with a SEIKO SPI-3800N probe station was employed at room temperature. A rectangle-shaped silicon tip was applied in dynamic force mode (DFM) experiments using a type of SI-DF3 with a spring force contact of 5 N m^{-1} and scan rates of 0.6 Hz.

Results and Discussion

Slow Self-Assembly of PS-Rich PS−PLLA BCP* in Solution. A selective solvent or even a nonsolvent can be introduced into BCP* solution to increase immiscibility between polymer and solvent so as to facile aggregation and self-assembly for ordering. The selective solvent or nonsolvent acts as a precipitant when added to a BCP solution in a good solvent. Self-assembly takes place at some critical selective or nonsolvent content. As shown in Figure 1a, lozenge-shaped single crystals with spiral dislocations are formed after addition of the nonsolvent (water) through slow self-assembly. Figure 1b shows the corresponding selected area electron

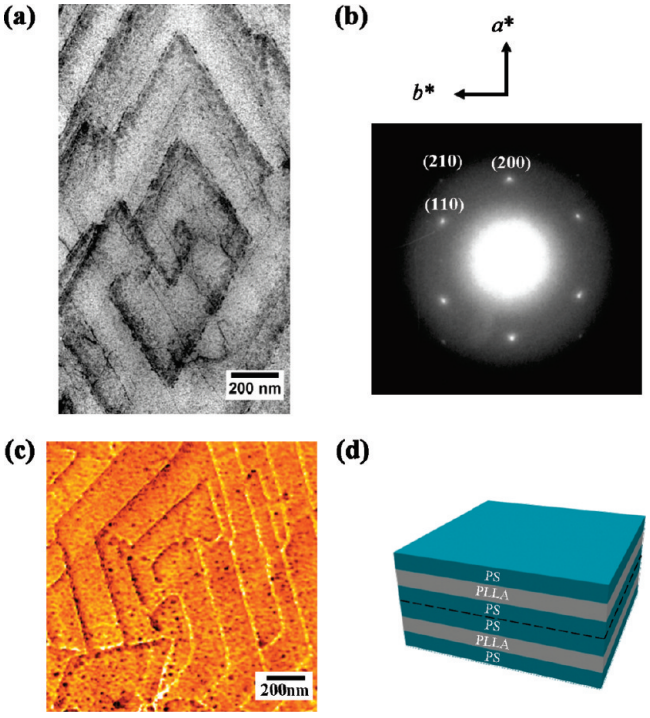

Figure 1. (a) TEM image and (b) corresponding SAED pattern of PS-rich PS−PLLA single crystals from the slow self-assembly. PS blocks are stained with RuO_4 to enhance mass−thickness contrast under TEM observation. (c) Tapping-mode SPM phase image of PS-rich PS−PLLA single crystals. (d) Illustration of PS-rich PS−PLLA layer-by-layer stacked single crystals and screw dislocations.

diffraction (SAED) pattern. It is the [001] zone pattern of the orthorhombic lattice of α-form.[46,47] A significant *hk*0 reflection of the PLLA unit cell can be found in the ED pattern, which confirms that the ED pattern is a projection along the *c*-axis. The PS-rich PS−PLLA single crystals have their molecular chains (i.e., *c*-axis) perpendicular to the substrate. The angles between growth faces are 60° and 120° (Figure 1a,c), indicating that the {110} faces are growth planes.[46,48−52] It is known that semicrystalline diblock copolymers, such as PS−PLLA and poly(styrene)-*b*-poly(ethylene oxide) (PS−PEO) diblock copolymers, can grow as single crystals in dilute solution under appropriate growth conditions. The PS−PLLA single crystal is a "sandwich" texture with the PLLA core covered by two PS block layers.[53] The lozenge-shaped PS−PLLA single crystals with spiral dislocations (Figure 1a,c) are layer-by-layer structures (Figure 1d) in which PLLA chains crystallize first, and the PS chains are rejected to allocate on the upper and lower surfaces of the PLLA lamellae. Furthermore, the result of the ED pattern (Figure 1b) indicates that chain directions in both layer-by-layer crystals are indeed parallel to their lamellar surface normal. The tapping mode SPM images (Figure 1c and Figure S2) further illustrate the observed morphologies and help determine the overall lamellar thickness (Figure S2). Partition between PLLA single-crystal thickness (d_{PLLA}) and PS amorphous thickness (d_{PS}) can be performed using the following approximation:[53] $d_{PLLA} = d_{overall}V_{PLLA}$ and $V_{PLLA} = [(M_n^{PLLA}/\rho_{PLLA})/(M_n^{PLLA}/\rho_{PLLA} + M_n^{PS}/\rho_{PS})]$, where M_n^{PLLA} and M_n^{PS} are the molecular weights of crystallizable PLLA and amorphous PS blocks and ρ_{PLLA} and ρ_{PS} are the densities of crystallizable PLLA and amorphous PS blocks, respectively, and V_{PLLA} and V_{PS} are the volume fractions of crystallizable PLLA and amorphous PS blocks. d_{PLLA} is found to be 6.7−7.6 nm by assuming ρ_{PLLA} is 1.28 g/cm^3 and ρ_{PS} is 1.052 g/cm^3,

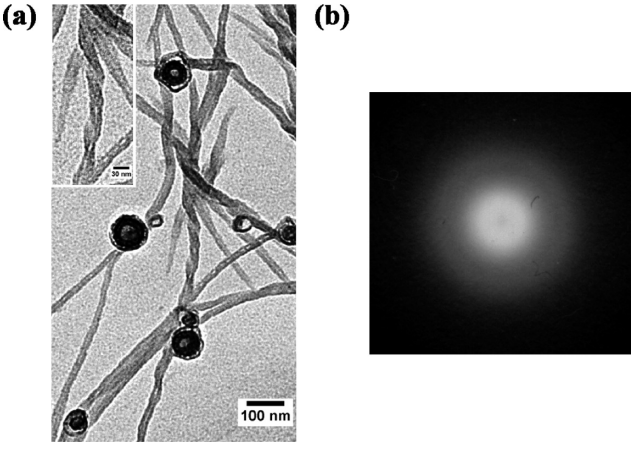

Figure 2. (a) TEM image and (b) corresponding SAED pattern of PS-rich PS−PLLA helical ribbon and tubular superstructure from the fast self-assembly. PS blocks are stained with RuO_4 to enhance mass−thickness contrast under TEM observation.

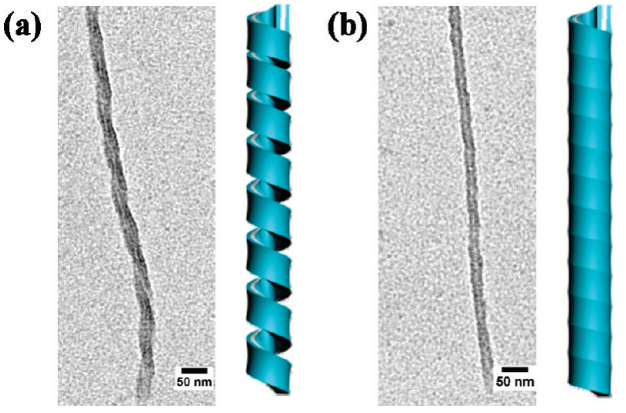

Figure 3. TEM images of (a) helical ribbon and (b) tubular superstructure with helical sense from the fast self-assembly of PS-rich PS−PLLA BCP* after sonication. PS blocks are stained with RuO_4 to enhance mass−thickness contrast under TEM observation.

respectively. The d_{PS} is equal to $(d_{overall} - d_{PLLA})/2$ and to be 6.65−7.7 nm. The experimentally estimated d_{PLLA} is approximately in line with the predicted value (~7.9 nm).[53] Moreover, the thickness of the layer-by-layer structure with the "sandwiched" texture is approximately in line with that measured by SPM. Consequently, the results indicate that PS-rich PS−PLLA single crystals can be obtained via slow addition of water to the BCP* solution. Clearly, the crystallization process takes place before the microphase separation and dominates the self-assembly process.

Fast Self-Assembly of PS-Rich PS−PLLA BCP* in Solution. In contrast to the slow self-assembly, rapid addition of water expedites the aggregation via a self-assembly process. Helical ribbons (inset of Figure 2a) and tubular superstructures are obtained (Figure 2a). No PS−PLLA single crystals are found. Occasionally, some micelles can also be observed as shown in Figure 2a. These micelles may have formed upon the addition of excess water to reach the cmc. Furthermore, as shown in Figure 2b, which is the SAED pattern of corresponding to Figure 2a, only amorphous diffused ring pattern of PS blocks are obtained. The helical ribbons and tubular superstructures are amorphous. No significant crystallization of PLLA takes place during the fast self-assembly.

The coexistence of amorphous helical ribbons and tubular superstructures may result from the fact that that the latter tubules (Figure 2a) result from tight scrolling of the helical

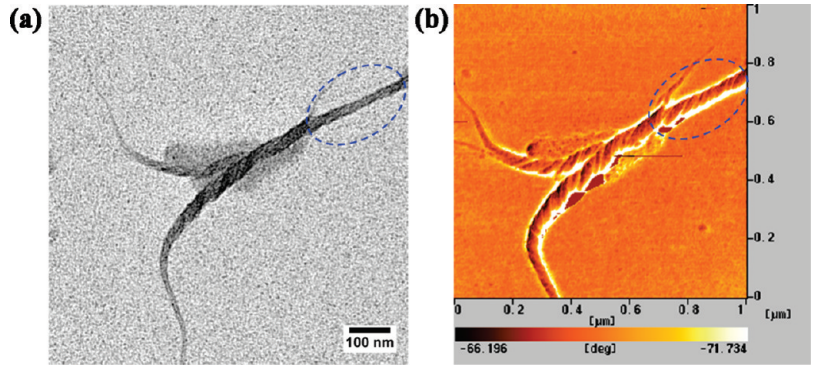

Figure 4. (a) TEM and (b) tapping-mode SPM phase images from the fast self-assembly of PS-rich PS−PLLA after sonication. PS blocks are stained with RuO_4 to enhance mass−thickness contrast under TEM observation. TEM and tapping-mode SPM phase images are taken from corresponding PS-rich PS−PLLA texture.

ribbons. To test this hypothesis, the solution from the fast self-assembly was sonicated to disperse the superstructures into isolate individual entities. As shown in Figure 3, well-distributed single helical ribbons (Figure 3a) and tubules (Figure 3b) are observed after sonication. The tubule in Figure 3b is actually the 2D projection of a tightly scrolled helical ribbon. However, the scrolling cannot be clearly observed under TEM due to contrast limitation of the 2D TEM projection. The same texture was therefore also investigated by tapping-mode SPM. As shown in Figure 4b, the central helical ribbon projection image under TEM (Figure 4a) also appears as a helical ribbon in tapping-mode SPM phase image (Figure 4b). By contrast, the upper right tubelike projection under TEM (marked inside the blue dashed line ellipse in Figure 4a) presents as tightly scrolled helix in tapping-mode SPM phase image (also inside the blue dashed line ellipse in Figure 4b). The data suggest that the tubular texture indeed results from the scrolling of helical ribbons.

The formation of the helical ribbons and helical tubules via fast self-assembly through microphase separation can be rationalized on the basis of TCLB (tilted chiral lipid bilayers) theory. According to the TCLB theory, the chirality driven microphase-separated helical ribbons and tubules with helical sense result from a compensation between incompatibility and specific interaction of chiral entities. Chirality driven hierarchical structures resulting from the self-assembly of chiral lipid bilayer molecules in solution (e.g., winding ribbon helices and tubular superstructures with helical sense) have been observed[54,55] and analyzed.[56−58] The chiral effect seems to be the major factor for the formation of helical ribbons. The formation of helices is driven by both intrinsic bending and twisting forces due to molecular chirality.[59] In a similar way, the present helical ribbons result from chirality driven twisting and bending of PS-rich PS−PLLA microphase-separated bilayers (see below for a detailed discussion). Furthermore, the transition from wounding ribbon helices to tubules with helical sense in solution can be observed.[54,55] The helical tubules are identified as the most stable superstructures, and they result from the scrolling of single-stranded helical ribbons.[56−58] The tubules reflect the chirality driven twisting and bending of bilayers through the scrolling of helical ribbons. PS-rich PS−PLLA amorphous helical ribbons and tubules with helical sense can be obtained via fast addition of water into BCP* solution to induce the self-assembly of PS-rich PS−PLLA BCP* chains via microphase separation. Namely, the microphase separation precedes crystallization and dominates the self-assembly of PS-rich PS−PLLA BCP* in solution through fast self-assembly.

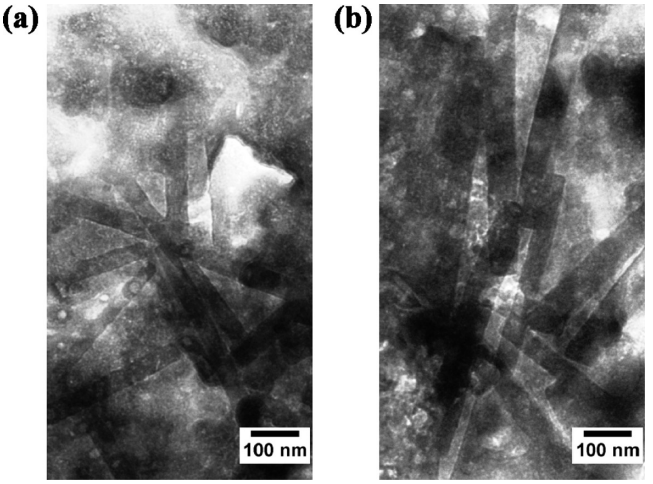

Figure 5. TEM images of flat ribbon superstructures from the (a) slow and (b) fast self-assembly of PS−PLA achiral BCP.

Self-Assembly of PS−PLA Achiral BCP in Solution. To further investigate the chiral effect on the self-assembly of BCP* in solution, the self-assembly of PS−PLA achiral BCP (i.e., PS355-PLA112 with $f_{PLA}^{v} = 0.27$) was carried out. As shown in Figure 5, regardless of the control of nonsolvent addition rate, the morphologies from the slow (Figure 5a) and fast (Figure 5b) self-assembly are in both cases flat ribbons. Their width is in line with the dimensions of the helical ribbons shown in Figures 2a and 3a. Since PS−PLA achiral BCP is noncrystallizable, the microphase separation dominates both the slow and the fast self-assembly processes. Also, the twisting and bending forces resulting from the packing of chiral molecules are not operative in the PS−PLA achiral BCP. As a result, flat ribbons instead of helical ribbons are formed. This also demonstrates that chirality indeed plays a major role in the formation of the helical ribbons during microphase separation.

Competition between Self-Assembly Processes: Crystallization and Microphase Separation. Single-crystal lozenge lamellae and amorphous helical ribbons were obtained via the slow and fast self-assembly of PS-rich PS−PLLA BCP* in solution, respectively. Both morphologies are the consequence of the competition between crystallization and microphase separation, as controlled by the nonsolvent addition rate. As illustrated in Figure 6, PS-rich PS−PLLA BCP* chains behave as isolated BCP* chains under dilute concentration in a good solvent (THF). Upon addition of the nonsolvent (water) into the BCP* solution, the isolated BCP*

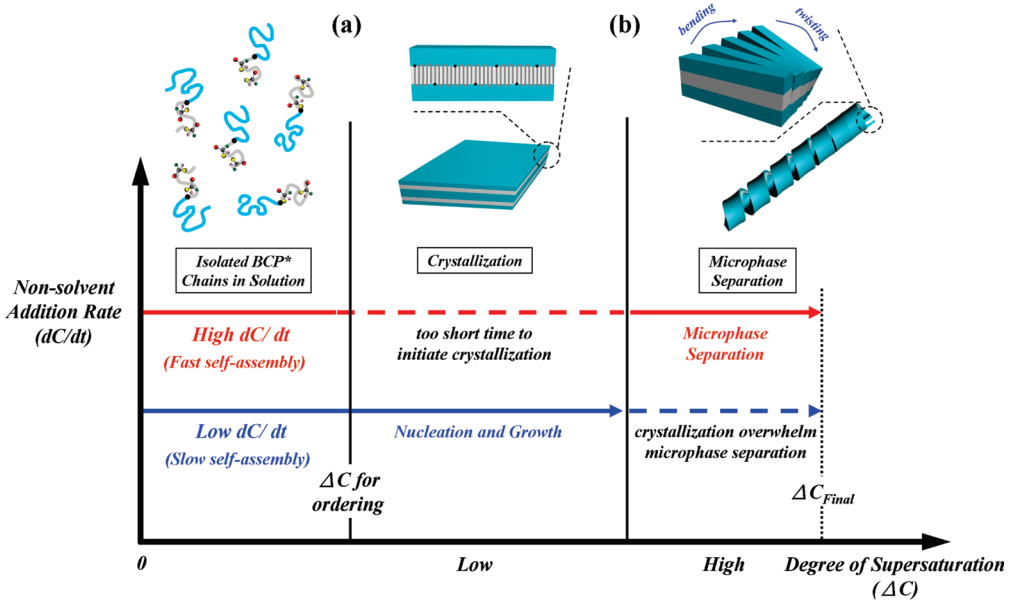

Figure 6. Illustration of PS-rich PS−PLLA BCP* chains in THF as the initial state and molecular dispositions of (a) single crystals from the slow self-assembly for crystallization and (b) microphase-separated helical ribbon superstructure from the fast self-assembly. The dashed line indicates that the nonsolvent addition rate is not suitable to achieve the self-assembly process for the formation of the superstructures under the reaching degree of supersaturation whereas the solid line suggests that the self-assembly process for the formation of preferential superstructures could be acquired by such nonsolvent addition rate. Note that PS-rich PS−PLLA BCP* chains with helical chain conformation lead to the twisting and bending of bilayered superstructures.

chains aggregate because of the increase of local BCP* concentration. Once the critical concentration for ordering is reached locally, crystallization or microphase separation takes place.

For the slow self-assembly, because of slow nonsolvent addition rate, local BCP* concentration near the aggregates increases slowly, and eventually BCP* in solution would be precipitated and the morphology is frozen because of the introduction of a large amount of nonsolvent. Accordingly, for the slow self-assembly, the self-assembly for ordering may involve a long relaxation process before solidification so as to experience a large range of the supersaturation (Figure 6a). Consequently, the crystallization of the BCP* may occur because of longer resident time at low supersaturation region. It is also noted that crystallization event usually overwhelm microphase separation from self-assembly. As a result, crystallization dominates the morphological evolution in the slow self-assembly. By contrast, for the fast self-assembly, the local BCP* concentration increases drastically before solidification so that high supersaturation can be reached in a short time (Figure 6b). The self-assembly only experiences short residence time in the low supersaturation region. As a result, time is too short to initiate the crystallization event, in particular because the crystallization rate of PLLA block in BCP* is significantly reduced by the noncrystallizable PS block (see below for reasons). The supersaturation quickly reaches a high level, and the corresponding concentration fluctuations are sufficient to induce microphase separation. Moreover, no morphological transitions (i.e., from a helical ribbons to a lozenge single-crystal lamellae) were found in the aggregates from the fast self-assembly even for a long period of time (more than 2 weeks) at ambient condition, indicating that once the helical ribbons are formed by the fast self-assembly, their structures may become "frozen in" due to the vitrification of the PS block ($T_{g,PS} \sim 100$ °C).

Self-Assembly of PLLA-Rich PS−PLLA BCP* in Solution. In comparison with PS-rich PS−PLLA BCP*, PS−PLLA BCP* with short PS chain (i.e., PLLA-rich PS−PLLA of

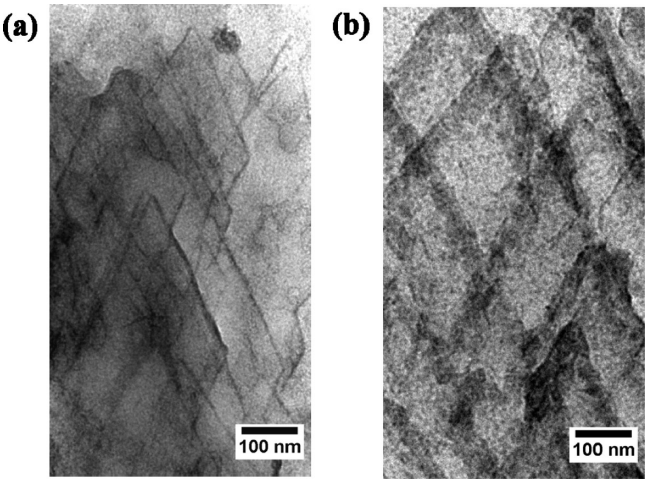

Figure 7. TEM images from (a) slow and (b) fast self-assembly of PLLA-rich PS−PLLA BCP*. PS blocks are stained with RuO_4 to enhance contrast under TEM observation.

PS55-PLLA95 with $f_{PLLA}^{v} = 0.65$) that comprise similar molecular weight of PLLA but smaller molecular weight of PS was synthesized to verify the model and to examine the composition effect on the self-assembly of PS−PLLA BCPs* in solution. As shown in Figure 7a, single-crystal lamellae were formed from the slow self-assembly of PLLA-rich PS−PLLA BCP*, which is identical to the morphologies from the slow self-assembly of PS-rich PS−PLLA BCP*. Single-crystal lamellae, instead of helical ribbons, are also found in the fast self-assembly case (Figure 7b). It appears that the composition changes the crystallization rate. Because crystallizable PLLA block is chemically connected to PS block, PLLA crystallization rate is strongly dependent on the molecular weight of PS block. The exclusion of amorphous blocks in the crystallization of semicrystalline BCP significantly affects the crystallization rate.[62] In the present

case, the shorter PS chain results in an increase of the crystallization rate of PLLA. PLLA crystallization dominates even the fast self-assembly, and only single-crystal lamellae are formed.

Conclusions

The competition between crystallization and microphase separation in the self-assembly of semicrystalline PS−PLLA BCPs* in solution was investigated by varying the nonsolvent addition rate. Single-crystal lozenge lamellae are obtained from the slow self-assembly of PS−PLLA BCP* with long PS chain (i.e., PS-rich PS−PLLA). Amorphous helical ribbons were obtained from the fast self-assembly. When supersaturation is approached slowly, nucleation and growth of PS-rich PS−PLLA BCP* single crystal takes place. By contrast, for the fast self-assembly, a high local concentration of semicrystalline PS-rich PS−PLLA BCP* chains (i.e., high aggregation rate) is reached. The microphase separation in a short time induces the formation of amorphous helical ribbons. Amorphous flat ribbons are formed from the self-assembly of PS−PLA achiral BCP regardless of the nonsolvent addition rate. Chirality indeed plays an important role in the formation of helical ribbons during microphase separation. By contrast, the formation of self-assembled morphologies of PS−PLLA BCP* with short PS chain (i.e., PLLA-rich PS−PLLA) in solution is dominated by PLLA crystallization regardless of the nonsolvent addition rate. The formation of helical architectures from the self-assembly of PS−PLLA BCP* reflects the impact of chirality from microphase separation, but the chiral effect may be overwhelmed by crystallization.

Acknowledgment. We thank Prof. S. Z. D. Cheng of Institute of Polymer Science of University of Akron for helpful discussions. This work is supported by the Taiwanese National Science Council (NSC97-2120-M-007-013).

Supporting Information Available: Initial morphologies of PS-rich and PLLA-rich PS−PLLA BCPs* in solution. This material is available free of charge via the Internet at http://pubs.acs.org.

References and Notes

(1) Bates, F. S.; Fredrickson, G. H. *Annu. Rev. Phys. Chem.* **1990**, *41*, 525–557.
(2) Matsen, M. W.; Schick, M. *Phys. Rev. Lett.* **1994**, *72*, 2660–2663.
(3) Bates, F. S.; Fredrickson, G. H. *Phys Today* **1999**, *52*, 32–38.
(4) Park, C.; Yoon, J.; Thomas, E. L. *Polymer* **2003**, *44*, 6725–6760.
(5) Yu, Y.; Eisenberg, A. *J. Am. Chem. Soc.* **1997**, *119*, 8383–8384.
(6) Shen, H.; Eisenberg, A. *J. Phys. Chem. B* **1999**, *103*, 9473–9487.
(7) Discher, D. E.; Eisenberg, A. *Science* **2002**, *297*, 967–973.
(8) Soo, P. L.; Eisenberg, A. *J. Polym. Sci., Part B: Polym. Phys.* **2004**, *42*, 923–938.
(9) Chastek, T. Q.; Lodge, T. P. *Macromolecules* **2004**, *37*, 4891–4899.
(10) Abbas, S.; Li, Z.; Hassan, H.; Lodge, T. P. *Macromolecules* **2007**, *40*, 4048–4052.
(11) Cornelissen, J. J. L. M.; Donners, J. J. J. M.; Gelder, R. E.; Graswinckel, W. S.; Metselaar, G. A.; Rowan, A. E.; Sommerdijk, N. A. J. M.; Nolte, R. J. M. *Science* **2001**, *293*, 676–680.
(12) Nelson, J. C.; Saven, J. G.; Moore, J. S.; Wolynes, P. G. *Science* **1997**, *277*, 1793–1796.
(13) Lokey, R. S.; Iverson, B. L. *Nature* **1995**, *375*, 303–305.
(14) Berl, V.; Huc, I.; Khoury, R. G.; Krische, M. J.; Lehn, J.-M. *Nature* **2000**, *407*, 720–723.
(15) Sone, E. D.; Zubarev, E. R.; Stupp, S. I. *Angew. Chem., Int. Ed.* **2002**, *41*, 1705–1709.
(16) Li, C. Y.; Cheng, S. Z. D.; Ge, J. J.; Bai, F.; Zhang, J. Z.; Mann, I. K.; Harris, F. W.; Chien, L.-C.; Yan, D.; He, T.; Lotz, B. *Phys. Rev. Lett.* **1999**, *83*, 4558–4561.
(17) Stadler, R.; Auschra, C.; Beckmann, J.; Krappe, U.; Voigt-Martin, I.; Leibler, L. *Macromolecules* **1995**, *28*, 3080–3097.
(18) Sakurai, S-.I.; Kuroyanagi, K.; Morino, K.; Kunitake, M.; Yashima, E. *Macromolecules* **2003**, *36*, 9670–9674.
(19) Cornelissen, J. J. L. M.; Fischer, M.; Sommerdijk, N. A. J. M.; Nolte, R. J. M. *Science* **1998**, *280*, 1427–1430.
(20) Ho, R.-M.; Chiang, Y.-W.; Tsai, C.-C.; Lin, C.-C.; Ko, B.-T.; Huang, B.-H. *J. Am. Chem. Soc.* **2004**, *126*, 2704–2705.
(21) Ho, R.-M.; Chen, C.-K.; Chiang, Y.-W.; Ko, B.-T.; Lin, C.-C. *Adv. Mater.* **2006**, *18*, 2355–2358.
(22) Ho, R.-M.; Chiang, Y.-W.; Chen, C.-K.; Wang, H.-W.; Hasegawa, H.; Akasaka, S.; Thomas, E. L.; Burger, C.; Hsiao, B. S. *J. Am. Chem. Soc.* **2009**, *131*, 18533–18542.
(23) Chiang, Y.-W.; Ho, R.-M.; Ko, B.-T.; Lin, C.-C. *Angew. Chem., Int. Ed.* **2005**, *44*, 7969–7972.
(24) Chiang, Y.-W.; Ho, R.-M.; Thomas, E. L.; Burger, C.; Hsiao, B. S. *Adv. Funct. Mater.* **2009**, *19*, 448–459.
(25) Douzinas, K. C.; Cohen, R. E. *Macromolecules* **1992**, *25*, 5030–5035.
(26) Cohen, R. E.; Bellare, A.; Drzewinski, M. A. *Macromolecules* **1994**, *27*, 2321–2323.
(27) Ryan, A. J.; Hamley, I. W.; Bras, W.; Bates, F. S. *Macromolecules* **1995**, *28*, 3860–3868.
(28) Hamley, I. W.; Fairclough, J. P. A.; Terrill, N. J.; Ryan, A. J.; Lipic, P. M.; Bates, F. S.; Towns-Andrews, E. *Macromolecules* **1996**, *29*, 8835–8843.
(29) Reiter, G.; Castelein, G.; Hoerner, P.; Riess, G.; Blumen, A.; Sommer, J.-U. *Phys. Rev. Lett.* **1999**, *83*, 3844–3847.
(30) Zhu, L.; Cheng, S. Z. D.; Calhoun, B. H.; Ge, Q.; Quirk, R. P.; Thomas, E. L.; Hsiao, B. S.; Yeh, F.; Lotz, B. *J. Am. Chem. Soc.* **2000**, *122*, 5957–5967.
(31) Reiter, G.; Castelein, G.; Sommer, J.-U.; Röttele, A.; Thurn-Albrecht, T. *Phys. Rev. Lett.* **2001**, *87*, 226101−1–226101−4.
(32) Chen, H.-L.; Hsiao, S.-C.; Lin, T.-L.; Yamauchi, K.; Hasegawa, H.; Hashimoto, T. *Macromolecules* **2001**, *34*, 671–674.
(33) Loo, Y.-L.; Register, R. A.; Ryan, A. J.; Dee, G. T. *Macromolecules* **2001**, *34*, 8968–8977.
(34) Loo, Y.-L.; Register, R. A.; Ryan, A. J. *Macromolecules* **2002**, *35*, 2365–2374.
(35) Zhu, L.; Cheng, S. Z. D.; Huang, P.; Ge, Q.; Quirk, R. P.; Thomas, E. L.; Lotz, B.; Hsiao, B. S.; Yeh, F.; Liu, L. *Adv. Mater.* **2002**, *14*, 31–34.
(36) Li, L.; Séréro, Y.; Koch, M. H. J.; Jeu, W. H. *Macromolecules* **2003**, *36*, 529–532.
(37) Balsamo, V.; Gil, G.; Navarro, U.; Hamley, I. W.; Gyldenfeldt, F.; Abetz, V.; Cañizales, E. *Macromolecules* **2003**, *36*, 4515–4525.
(38) Ho, R.-M.; Lin, F.-H.; Tsai, C.-C.; Lin, C.-C.; Ko, B.-T.; Hsiao, B. S.; Sics, I. *Macromolecules* **2004**, *37*, 5985–5994.
(39) Ho, R.-M.; Chung, T.-M.; Tsai, J.-C.; Kuo, J.-C.; Hsiao, B. S.; Sics, I. *Macromol. Rapid Commun.* **2005**, *26*, 107–111.
(40) Koo, C. M.; Wu, L.; Lim, L. S.; Mahanthappa, M. K.; Hillmyer, M. A.; Bates, F. S. *Macromolecules* **2005**, *38*, 6090–6098.
(41) Sun, Y.-S.; Chung, T.-M.; Li, Y.-J.; Ho, R.-M.; Ko, B.-T.; Jeng, U.-S.; Lotz, B. *Macromolecules* **2006**, *39*, 5782–5788.
(42) Castillo, R. V.; Muller, A. J.; Lin, M.-C.; Chen, H.-L.; Jeng, U.-S.; Hillmyer, M. A. *Macromolecules* **2008**, *41*, 6154–6164.
(43) Mark, J. E. *Physical Properties of Polymers Handbook*; AIP Press: New York, 1996.
(44) Grulke, E. A. Solubility Parameters Values. In *Polymer Handbook*; Brandrup, J., Immergut, E. H., Eds.; Wiley: New York, 1989; Vol. *VII*, p 519 ff.
(45) Brandrup, J.; Immergut, E. H. *Polymer Handbook*; Wiley: New York, 1989.
(46) Miyata, T.; Masuko, T. *Polymer* **1997**, *38*, 4003–4009.
(47) Cartier, L.; Okihara, T.; Lotz, B. *Macromolecules* **1997**, *30*, 6313–6322.
(48) Reneker, D. H.; Geil, P. H. *J. Appl. Phys.* **1960**, *31*, 1916–1925.
(49) Kalb, B.; Pennings, A. J. *Polymer* **1980**, *21*, 607–612.
(50) Hoogsteen, W.; Postema, A. R.; Pennings, A. J.; ten Brinke, G.; Zugenmaier, P. *Macromolecules* **1990**, *23*, 634–642.
(51) Kobayashi, J.; Asahi, T.; Ichiki, M.; Oikawa, A.; Suzuki, H.; Watanabe, T.; Fukada, E.; Shikinami, Y. *J. Appl. Phys.* **1995**, *77*, 2957–2973.
(52) Iwata, T.; Doi, Y. *Macromolecules* **1998**, *31*, 2461–2467.
(53) Zheng, J. X.; Xiong, H.; Chen, W. Y.; Lee, K.; Van Horn, R. M.; Quirk, R. P.; Lotz, B.; Thomas, E. L.; Shi, A.-C.; Cheng, S. Z. D. *Macromolecules* **2006**, *39*, 641–650.
(54) Nakashima, N.; Asakuma, S.; Kunitake, T. *J. Am. Chem. Soc.* **1985**, *107*, 509–510.

(55) Fuhrhop, J.-H.; Schnieder, P.; Boekema, E.; Helfrich, W. *J. Am. Chem. Soc*. **1988**, *110*, 2861–2867.
(56) Zhong-can, O.-Y.; Jixing, L. *Phys. Rev. Lett*. **1990**, *65*, 1679–1682.
(57) Zhong-can, O.-Y.; Jixing, L. *Phys. Rev. A* **1991**, *43*, 6826–6836.
(58) Selinger, J. V.; Schnur, J. M. *Phys. Rev. Lett*. **1993**, *71*, 4091–4094.
(59) Nandi, N.; Bagchi, B. *J. Am. Chem. Soc*. **1996**, *118*, 11208–11216.
(60) Hashimoto, T. *Macromolecules* **1987**, *20*, 465–468.
(61) Fredrickson, G. H.; Binder, K. *J. Chem. Phys*. **1989**, *91*, 7265–7275.
(62) Heuschen, J.; Jérôme, R.; Teyssié, P. H. *J. Polym. Sci., Part B: Polym. Phys*. **1989**, *27*, 523–544.